Z. Kristallogr. Proc. **1** (2011) 241-246 / **DOI** 10.1524/zkpr.2011.0036
© by Oldenbourg Wissenschaftsverlag, München

Compression and thermal expansion of nanocrystalline TiN

S. Stelmakh[1,*], E. Grzanka[1], S. Gierlotka[1], J. F. Janik[2], M. Drygaś[2], C. Lathe[3], B. Palosz[1]

[1] Institute of High Pressure Physics, Polish Academy of Sciences, Warsaw, Poland
[2] AGH University of Science and Technology, Faculty of Energy and Fuels, Krakow, Poland
[3] GeoForschungsZentrum Potsdam, Potsdam, Germany
[*] Contact author; e-mail: svrit@unipress.waw.pl

Keywords: TiN, nanocrystals, high pressure, high temperature

Abstract. TiN nanopowders synthesized by the application of an anaerobic „imide" route and aerosol synthesis with 5 and 26 nm average size were examined by in situ diffraction at high pressure up to 6 GPa and high temperature up to 800°C. Overall compressibilities and thermal expansion coefficients were determined for the examined pressure and temperature intervals. Nanocrystals of TiN show core-shell type structure where elastic properties of interior and surface shell are different; surface is softer and shows larger thermal expansion than crystalline TiN. Core-shell model was confirmed by analysis of large Q powder diffraction at room temperature with application of *alp*-Q and PDF analysis.

1. Introduction

Titanium nitride TiN is an important material with diverse application potentials due to its unique properties [1, 2] (*e.g.*, electrical conductivity comparable with that of Ti metal, high melting point of about 3000 °C, very high hardness, significant chemical corrosion resistance, golden color in thin films). There are numerous methods available for the preparation of both powders and thin films of TiN [3, 4]. They include the conventional methods of nitridation of Ti metal or TiH_2 with various nitrogen sources, carbothermal reduction/nitridation of microcrystalline TiO_2, and CVD methods utilizing certain volatile Ti precursors (*e.g.*, $TiCl_4$, $Ti[N(CH_3)_2]_4$). Typically, these approaches yield microcrystalline TiN due to the high temperatures required to complete the nitridation reactions, especially, if oxygen bearing precursors are used. There are also reports describing the preparation of nanocrystalline powders of TiN; they include a laser ablation method, ammonolysis of $TiCl_4$, direct nitridation of nanocrystalline TiO_2 (preformed or carried out *in situ*), and metathesis reactions of $TiCl_4$ and NaN_3 or $NaNH_2$.
Under ambient conditions TiN shows a stable cubic lattice labeled as c-TiN. It appears that the powders of this nitride (including nanopowders) can only be sintered with difficulty by the application of field-assisted or spark plasma sintering conditions [5] or under non-isothermal conditions up to 1500 ºC which yield high oxygen-content TiN ceramics [6]. No known reports address sintering of nano-TiN under HP-HT conditions.

The TiN nanopowders used in this study were synthesized by an anaerobic route *via* the reaction of $Ti[N(CH_3)_2]_4$ with liquid ammonia at -33 °C followed by the pyrolysis of the resulting Ti-imide precursor under a flowing ammonia gas at 500 °C or 800 °C [7, 8]. The brown product powders were found by powder XRD in each case to be phase pure nanocrystalline c-TiN with an average crystallite size of 5 nm and 26 nm, respectively. Upon preparation, the powders were sealed under vacuum in glass ampoules for further studies. The use of oxygen-free precursors coupled with stringent adherence to anaerobic conditions in this method (Schlenk technique) routinely results in materials with only residual oxygen contents, if any. No oxygen was found by chemical analysis in the Ti-imide precursor. The excess of ammonia applied at all stages creates advantageous conditions for the formation of oxygen-free stoichiometric TiN.
Preliminary studies on high-pressure sintering and recrystallization of nanocrystalline TiN were performed at HASYLAB, MAX80 Cubic Anvil Press (F2.1 station) to obtain high-density/low oxygen TiN ceramics [9]. In this article we present examination of two powders of TiN with the 5 nm and 26 nm average grain size prepared as described above. Generation and relaxation of micro-strains was traced by analyzing the macro-strain measured from weighted positions of Bragg reflections; micro-strain was traced by measuring FWHM of these reflections. The diffraction data were collected in energy dispersive geometry. Sodium chloride was applied as a pressure marker and no pressure medium was used.

2. Data analysis

2.1 Compression

Figure1 shows compression of TiN powders under the pressure of 0-6 GPa measured for (200) reflections. There are plotted values of relative interplanar spacings $(d/d_0)_{200}$, where d_0= 2.13Å and corresponds to crystalline TiN, and FWHMs measured for 200 reflection. The specific shape of the plots is due to a core-shell structure of individual grains [10]. Referring to such a model there are two distinctive volume fractions in a nanocrystalline sample which correspond to the core and the shell. In general, what one measures in an experiment as a single Bragg reflection is a combination of two sub-reflections corresponding to the core and shell of the grain for which one measures one average (weighted) position.
Figure 1 (a) shows that at ambient pressure, d_{200} values of both samples under examination are smaller than in bulk TiN by about 1%. (Note that the first measurements were performed on the samples already loaded in a high pressure container and pre-compressed so, there were already under pressure of about 0.5-1.0 GPa). At the initial stage of compression, up to about 2.5-3.0 GPa, the 5 nm sample compresses very strongly, and 26 nm sample shows no compression. At this stage, there is a strong increase of micro-strains in 5 nm sample but no increase of strains is observed in the 26 nm sample, fig. 1(b).
The origin of this behavior is in different elastic properties of cores and shells of the grains: softer shells and harder cores. Assuming that surface shell is about 0.5 nm thick (see Section 2.3), in 5 nm grain there is about 50% of atoms located at the surface, in 26 nm grain - about 10%. The pronounced compression of soft shells has a strong effect on the position of Bragg reflection of 5 nm sample, but only a little for 26 nm sample. Assuming that for material with a core-shell model each Bragg reflection is combined from two reflections, for 5 nm sample they are of similar intensity and that its position and width is a good volume average of the its structure. Situation is very different for 26 nm sample where grain cores constitute

90% of the sample volume and presence of only 10% of surface atoms has a little effect both on peak position and its FWHM. Referring to this analysis we propose a tentative interpretation of compression plots showed in figure 1. At the initial stage of compression most of the strain energy is accumulated in the shell which hardens and protects the inner part of the grains from being compressed [10]. The positions of Bragg reflections reflect average compression of core and shell for 5 nm sample, but for 26 nm sample they reflect compression and microstrain of the cores which form 90% of the sample volume. At the second stage, above 3 GPa, the material becomes homogenous (the densities of cores and shells become equal) and the measured compression of both samples is similar and corresponds to the elastic modulus of TiN lattice, $B_0 \cong 270$ GPa. At this stage FWHM (thus micro-strain) increases similarly for both materials, of about 0.02 [$Å^{-1}$]. Due to different elastic properties of the grain cores and shells, no single value of bulk modulus might be associated to given nanomaterial. However, it is worth to notice that in result of compression to 6 GPa the relative change of interplanar spacing $(d/d_0)_{200}$ increases with a decrease of the grain size; it is about 0.99 for crystalline, 0.985 for 26 nm and 0.975 for 5 nm sample. It might be interpreted as that nano-TiN is softer than crystalline material.

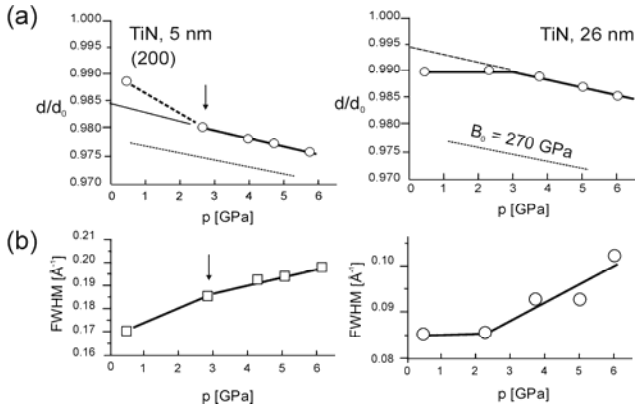

Figure 1. Compression of 5 and 26 nm TiN powders, (a), and corresponding changes of FWHM of (200) Bragg reflection, (b); instrumental line width is 0.03 [$Å^{-1}$].

2.2 Thermal expansion

Figure 2 shows that for the samples annealed under pressure, there is a characteristic temperature which divides the examined temperature interval in two parts where TiN shows different average thermal expansion. Up to temperature of about 500°C the thermal expansion coefficient is about that observed for single crystalline material; the inlet shows the lattice expansion corresponding to $\alpha = 9.5\ 10^{-6}\ K^{-1}$. Above 500°C the thermal expansion is larger, figure 2 (a), and this is accompanied by a very rapid relaxation of micro-strains, figure 2 (b). After full relaxation of micro-strains at about 800°C the material is fully dense and FWHM describes only grain size of the samples. During cooling, the decrease of lattice parameters follows thermal expansion coefficient. After release of the applied stress, at ambient conditions the relative d-spacings, d/d_0, measured for both samples are smaller than 1.0, what

indicates that average lattice of nanocrystalline samples is compressed in comparison with crystalline TiN; it is 0.99 and 0.995 for 5 and 26 nm samples.

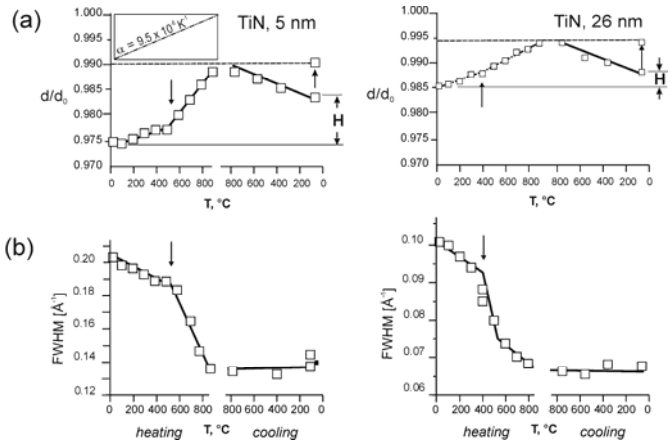

Figure 2. Thermal expansion of 5 and 26 nm TiN powders under pressure 6 GPa, (a), and corresponding changes of FWHM of (200) reflection, (b).

A "stepwise" character of thermal expansion showed by nanocrystalline TiN is obviously connected with a non-uniform structure of the grains. Taking into account that a nanocrystal shows a core-shell structure the volume fractions of the cores and shells contribute to Bragg maxima with adequate weights. The plots of figures 1 and 2 present average compression and average lattice expansion as measured from weighted positions of the reflections. A very "fast" relaxation above 400-500^{o}C observed in figure 2 (b) describes the process of redistribution of macro- and micro-strains, rearrangement of individual nanograins and disappearance of porosity in the material. After the process of annealing is completed at 800^{o}C, the material shrinks following bulk thermal expansion coefficient.

It is evident that, due to core-shell structure of examined nano-TiN, no single value of thermal expansion coefficient can be associated with specific sample. However, one may ask about an "overall thermal expansion" under given p-T conditions. For 5 and 26 nm samples which were measured under pressure of 6 GPa, for the temperature range 20-800^{o}C the corresponding values of "overall" α_T are $2*10^{-5}$ (0.990 - 0.975)/780 and $1.2*10^{-5}$ K^{-1} (0.995-985)/780. This is a clear indication of different thermal expansions of grain cores and shells.

2.3 Examination of core-shell structure with use of large-Q diffraction

Core-shell structure of nanocrystalline TiN was examined with use of large-Q x-ray measurements of up to Q < 25 Å^{-1} performed at room temperature at ESRF at Lens Assisted High Energy Diffraction, Station ID15A. Reciprocal space analysis was made with application of *alp* methodology and referred to a core-shell model [11]. Theoretical diffraction patterns were calculated for a series of models of 5 nm TiN grains with different thickness of the surface shell for both compressed and expanded surface shell. Experimental *alp* values were calculated for individual Bragg reflections but also for groups of overlapping reflections at larger Q's. In figure 3 there are plotted relative apparent lattice parameters, alp/a_0, where a_0 corresponds to lattice parameter of crystalline TiN, 4.242 Å [JPCDS Cards, No. 38-1420].

All experimental alp/a_0 values are smaller than 1 what means that "on average" inter-atomic distances (thus inter-atomic bonds) are shorter in nano- than in crystalline material. This conforms with high-pressure studies where as measured lattice parameters for nanocrystalline samples are by 0.5-1% smaller than for crystalline TiN. Figure 3 shows a comparison of experimental to theoretical *alp*-Q plots for best matched model with a tensile-type strain in the surface shell. Although "general shapes" of theoretical and experimental *alp*-*Q* dependencies match pretty well, there is a clear "dispersion" of individual experimental *alp* values about rather smooth theoretical plot. This shows that the core shell model which was applied with a radial strain in the shell is only approximate and requires further improvement.

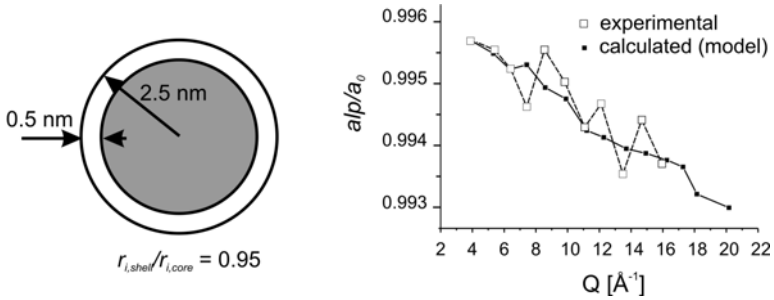

Figure 3. Experimental alp-Q plot of 5 nm TiN powders compared to alp-Q plot calculated for the core-shell model with 0.5 nm thick surface shell being under tensile-type strain of 5%.

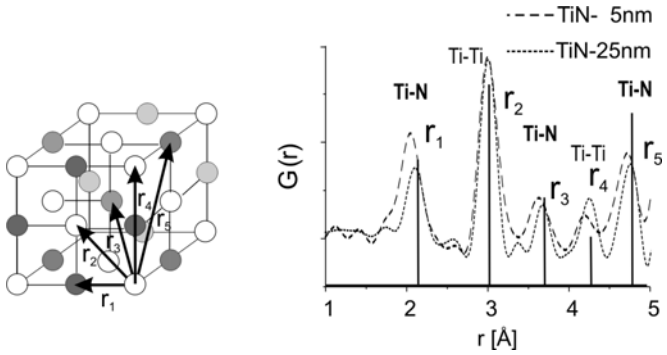

Figure 4. The first five inter-atomic distances in experimental PDF plot of 5 and 26 nm TiN powders.

PDF analysis (program PDFgetX2 [12]) was performed with use of same diffraction data as that used for *alp*-Q analysis. It showed that there is a clear decrease of all inter-atomic distances with a decrease in the grain size, figure 4. That, at first sight, shows that real and reciprocal space analyses are consistent: they both show a "overall" compression of the crystal lattice of TiN with a decrease of the grain size. PDF plot shows, however, that there is evident difference between size dependent decrease of even and odd *r*-values: *r*'s with even indexes correspond to Ti-Ti (N-N) and they shorten much less than Ti-N bonds, what means that relaxation in the surface shell occurs mostly though changes of Ti-N bonds with only little changes within Ti- and N-sublattices.

3. Summary

Examination of compression and thermal expansion of nanocrystalline TiN powders showed that overall compressibility of nano-TiN increases with a decrease of grain size and, thermal expansion increases. These overall parameters are valid for specific pressure and temperature intervals. The difference between compressibility and thermal expansion of crystalline and nano-crystalline materials results from different elastic properties of the interior and surface shell of individual nano-grains. From high pressure studies it was deduced that surface shell is "softer" than interior of the grains and, therefore the surface shell compresses more under pressure and expands more with an increase of temperature than the grain interior. Densities and elastic properties of grain core and shell become similar at pressure about 3 GPa. Under pressure 6 GPa relaxation of micro-strains begins at about 500^{o}C and it ends at about 800^{o}C for 5 nm and at about 600-700^{o}C for 26 nm powder. Reciprocal and real space analysis performed with use of large Q diffraction data gives a clear indication that nanocrystalline TiN shows a core shell structure with a tensile-type strain in the surface shell.

References

1. Chen, L.Y., Gu, Y.L., Shi, L., Ma, J.H., Yang, Z. & Qian, Y.T., 2004, *J. Nanosci. Nanotechnol.*, **4**, (7), 896-898.
2. Fix, R.M., Gordon, R.G. & Hoffman, D.M., 1990, *Chem. Mater.*, **2**, 235-241.
3. Drygas, M., Czosnek, C., Paine, R.T. & Janik, J.F., 2006, *Chem. Mater.*, **18**, 3122-3129 (and references therein).
4. Zukalova M., Prochazka J., Bastl Z., Duchoslaw J., Rubacek L., Havlicek D., Kavan L., 2010, *Chem. Mater.*, **22**, 4045-4055 (and references therein).
5. Wang L., Jiang W., Chen L., Yang M., Zhu H., 2006, *J. Am. Ceram. Soc.*, **89**, 2364-2366.
6. Zgalat-Lozinskii O. B., Bulanov V. N., Timofeeva I. I., Ragulya A. V., Skorokhod V. V., 2001, *Powder Metall. Metal. Ceram.,* **40**, 573-581.
7. Brown G. M., Maya L., 1988, *J. Am. Ceram. Soc.*, **71** (1), 78-82.
8. Drygaś, M., Czosnek C., Janik J. F., 2006, *Book of abstracts of NANOMAT 2006 – International Workshop on Nanostructured Materials*, *June 21-23, 2006 Antalya, Turkey*, 201.
9. Stelmakh, S., Grzanka, E., Gierlotka, S., Swiderska-Sroda, A., Palosz, B., Janik, J.F., Drygaś, M.& Lathe C., 2009, *HASYLAB Annual Report 2009.*
10. Palosz„B., Stelmakh, S., Grzanka, E., Gierlotka, S., Pielaszek, R., Bismayer, U., Werner, S.& Palosz, W., 2004, *J. Phys.: Condens Matter,* **16** *,* 353-377.
11. Palosz, B., Stelmakh, S., Grzanka, E., Gierlotka, S. & Palosz, W., 2007, *"Nanocrystallography", in: Z. Kristallogr.,* **222,** 580-594.
12. Qiu, X., Thompson, J.W. & Billinge, S.J.L., 2004, *J. Appl. Crystallogr.,* **37**, 678-678.

Acknowledgements. This work was supported by DESY-HASYLAB, Project I-20070111 EC, Contract RII3-CT-2004-506008 (IA-SFS) and ESRF, Project HS-3971. SS wants to thank Veijo Honkimaki for help with experiment on ID15A at ESRF. JFJ wants to acknowledge a financial support of MNiSW/AGH-UST (Poland), task No. 11.11.210.120.